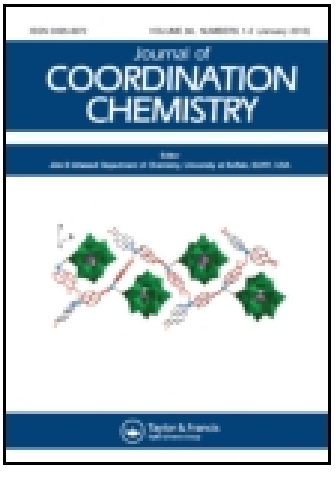

Journal of Coordination Chemistry
Publication details, including instructions for authors and subscription information:
http://www.tandfonline.com/loi/gcoo20

One-pot synthesis, structural elucidation, DNA binding and alkaline phosphatase inhibition studies of zinc(II) complexes with 4-nitrocinnamic acid and ethylenediamine

Syeda Tahira Hafeez[a], Saqib Ali[a], Muhammad Nawaz Tahir[b], Muhammad Iqbal[a] & Khurram Shahzad Munawar[a]

[a] Department of Chemistry, Quaid-I-Azam University, Islamabad, Pakistan

[b] Department of Physics, University of Sargodha, Sargodha, Pakistan

Accepted author version posted online: 04 Aug 2014.Published online: 14 Aug 2014.

To cite this article: Syeda Tahira Hafeez, Saqib Ali, Muhammad Nawaz Tahir, Muhammad Iqbal & Khurram Shahzad Munawar (2014) One-pot synthesis, structural elucidation, DNA binding and alkaline phosphatase inhibition studies of zinc(II) complexes with 4-nitrocinnamic acid and ethylenediamine, Journal of Coordination Chemistry, 67:14, 2479-2495, DOI: 10.1080/00958972.2014.940922

To link to this article: http://dx.doi.org/10.1080/00958972.2014.940922

Journal of Coordination Chemistry, 2014
Vol. 67, No. 14, 2479–2495, http://dx.doi.org/10.1080/00958972.2014.940922

One-pot synthesis, structural elucidation, DNA binding and alkaline phosphatase inhibition studies of zinc(II) complexes with 4-nitrocinnamic acid and ethylenediamine

SYEDA TAHIRA HAFEEZ†, SAQIB ALI*†, MUHAMMAD NAWAZ TAHIR‡, MUHAMMAD IQBAL† and KHURRAM SHAHZAD MUNAWAR†

†Department of Chemistry, Quaid-I-Azam University, Islamabad, Pakistan
‡Department of Physics, University of Sargodha, Sargodha, Pakistan

(*Received 2 January 2014; accepted 6 June 2014*)

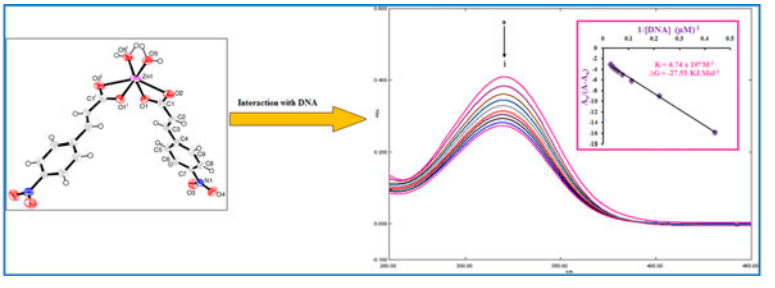

The synthesized compounds interact with DNA via intercalative mode of interaction.

We report one-pot synthesis of zinc(II) complexes with 4-nitrocinnamic acid (HL), $[ZnL_2(H_2O)_2]$ (**1**), $[ZnL_2(DMSO)_2]$ (**2**) and $[Zn(en)_2(H_2O)_2]L_2(H_2O)_2$ (**3**), where DMSO = dimethylsulfoxide and en = ethylenediamine. The complexes were prepared by reacting sodium 4-nitrocinnamate with zinc acetate in aqueous medium and characterized by FT-IR, NMR and single crystal X-ray diffraction. The results have shown distorted octahedral geometry for **1** and **3** while tetrahedral for **2** where the carboxylate coordinated bidentate and monodentate in **1** and **2** is uncoordinated in **3**, replaced completely by ethylenediamine. The complexes were also screened for their DNA interaction and alkaline phosphatase (ALP) inhibition using cyclic voltammetry, viscometry and UV–visible spectroscopy. All these techniques indicated strong electrostatic binding of the complexes with DNA. The diffusion coefficients of the complexes decreased on DNA addition indicating binding of the complexes with DNA. The binding constants were also calculated through CV and UV spectra. The complexes were screened for ALP inhibition activity as well, where 80% activity was found for **1**.

Keywords: Zn(II) complexes; Crystal structures; 4-nitrocinnamic acid; DNA binding; Alkaline phosphatase inhibition

*Corresponding author. Email: drsa54@yahoo.com

1. Introduction

Ligands containing carboxylate give complexes with interesting topologies and are therefore widely studied. Carboxylates show diverse binding geometries, such as monodentate, monodentate bridging, bidentate bridging and chelating [1, 2]. They also facilitate the synthesis of complexes with low coordination number but high stability, both with flexible and bulky ligands [1, 3, 4].

Cinnamic acids and their derivatives are ubiquitous in plant species and can be found in products such as fruits, vegetables, tobacco leaves, coffee beans, bee propolis, beer and wines [5, 6]. They possess pharmacological properties such as anti-oxidant, anti-diabetic and hepatoprotective [5, 7, 8]. They can scavenge free radicals providing protection against certain carcinogens, mutagens or atherosclerosis. Moreover, cinnamic acids are also used in the synthesis of flavonoids, a very large class of natural products [6].

We study the interaction of cinnamic acid with zinc, which is an essential element in human growth. Zinc is a constituent of more than 300 metalloenzymes and is a component of *zinc fingers*, which are the special proteins involved in safe transfer of genetic information [9–12]. Zinc also possesses antiviral, antibacterial and wound-healing properties. Moreover, zinc complexes are also used in the treatment of gastrointestinal disorders, acne therapy and infertility [9, 13].

Although zinc complexes are relatively less studied they are important in supramolecular chemistry and in biological systems. Mononuclear zinc complexes can mimic active sites of certain enzymes containing zinc binding sites and can serve as model complexes for research [1, 14]. Alkaline phosphatase (ALP) is a hydrolase enzyme and is involved in recycling of phosphate within living cells. Presence of zinc(II) ions causes deactivation of enzyme [15, 16]. Organic chelating ligands such as bidentate amines are used in mimic chemistry as substitutes for amino acid side groups and as model complexes to study non-covalent interactions in biological systems [17]. The interaction of such complexes with DNA is of interest, as they can recognize specific DNA sequence, alter local structure of DNA and affect gene-expression [18, 19]. The study of interaction with DNA finds application in designing new drugs, DNA foot printing and in DNA-dependent electron transfer reactions [20]. Non-redox active metals such as zinc(II) are important as their reactivity in the model systems can lead to functional DNA cleaving molecules [21].

In the present study we report synthesis, structural characterization, DNA binding and ALP inhibition studies of three new zinc(II) complexes with 4-nitrocinnamic acid. DNA binding study was conducted with viscometry, UV–visible spectroscopy and cyclic voltammetry. The values of DNA binding constant (K_b), Gibbs free energy change (ΔG) and diffusion coefficients (D_o) have been calculated. Inhibition activity of ALP by the synthesized complexes is also reported.

2. Experimental

2.1. *Materials*

$Zn(CH_3COO)_2{\cdot}2H_2O$, 4-nitrocinnamic acid, ethylenediamine, $NaCO_3$, $NaHCO_3$ and salmon sperm DNA (SSDNA) were obtained from Fluka, Switzerland. Methanol and DMSO were obtained from Merck, Germany and were used as such, without drying and further purification.

Singly distilled water was used as solvent for synthesis. *p*-Nitrophenyl phosphate hexahydrate (*p*-NPP) was purchased from Sigma Aldrich, USA. ALP was extracted from human serum.

2.2. *Physical measurements*

FT-IR spectra were recorded from 4000 to 400 cm^{-1} using a Nicolet-6700 FT-IR spectrophotometer. ^1H NMR spectra were recorded on a Bruker 300 MHz NMR spectrometer (Switzerland) at room temperature using DMSO-d_6 as an internal reference [δ ^1H (DMSO) = 2.5 and δ ^{13}C (DMSO) = 40 ppm]. X-ray single crystal analyses were collected on a Bruker Kappa APEX-II CCD diffractometer using graphite-monochromated Mo-Kα radiation ($\lambda = 0.71073$). The crystal structures were solved by direct methods followed by final refinement carried on F^2 with full-matrix least-squares using SHELXL-97 [22]. DNA binding studies were performed using UV–visible spectroscopy and enzyme inhibition studies were performed on a Beckman U-2020 spectrophotometer at 25 °C. For the cyclic voltammetric studies, a BioLogic SP-300 cyclic voltammeter was used, running with EC-Lab Express V 5.40 software, Japan.

2.3. *Procedures for the synthesis of 1–3*

2.3.1. $[ZnL_2(H_2O)_2]$ (1). Sodium salt of HL (4-nitrocinnamic acid) was prepared by dropwise addition of methanolic solution of ligand (0.58 g, 3 mM) to an aqueous solution of sodium bicarbonate (0.252 g, 3 mM) with constant stirring at 50 °C. After 2 h stirring, aqueous solution of zinc acetate dihydrate (0.329 g, 1.5 mM) was added dropwise. The reaction mixture was further stirred for 2 h at 50 °C. The final product was filtered, washed with distilled water, air dried and recrystallized in methanol. Yield: 81%, FT-IR (cm^{-1}): 1527 $\nu(OCO)_{asym}$, 1359 $\nu(OCO)_{sym}$, $\Delta\nu = 168$, 3450–2400 ν(O–H), 3081 ν(Ar–H), 1634 ν(C=C), 1486, 1336 ν(NO2), 425 ν(Zn–O).

2.3.2. $[ZnL_2(DMSO)_2]$ (2). Complex **2** was prepared by dissolving the air dried product obtained for **1** in DMSO followed by slight heating of the solution. The clear solution was placed for crystallization where faint yellow crystals of **2** were formed. Yield: 73%, FT-IR (cm^{-1}): 1599 $\nu(OCO)_{asym}$, 1364 $\nu(OCO)_{sym}$, $\Delta\nu = 235$, 3003 ν(Ar–H), 1645 ν(C=C), 1412, 1339 ν(NO2), 420 ν(Zn–O).

2.3.3. $[Zn(en)_2(H_2O)_2]L_2(H_2O)_2$ (3). Sodium salt of HL was prepared by same procedure as for **1**. After 2 h stirring, aqueous solution of zinc acetate dihydrate (0.329 g, 1.5 mM) was added dropwise. After further stirring of 2 h, ethylenediamine (0.1 mL, 1.5 mM) was added. Reaction mixture was further stirred for 3–4 h under the same reaction conditions. The solvent was rotary evaporated and the dried product was recrystallized in water. Yield: 60%, FT-IR (cm^{-1}): 1548 $\nu(OCO)_{asym}$, 1371 $\nu(OCO)_{sym}$, $\Delta\nu = 177$, 3500–2450 ν(O–H), 3043 ν(Ar–H), 1642 ν(C=C), 1492, 1412 ν(NO2), 508 ν(Zn–N), 425 ν(Zn–O).

2.4. *DNA interaction studies by viscosity measurements*

Viscosity measurements were performed at room temperature (25 ± 1 °C) using a Ubbelohde viscometer. Digital stopwatch was used to measure the flow time. The average flow time

was measured from triplicate measurements. Between the successive measurements, the viscometer was rinsed with acetone and air dried. Data were presented as plots of relative viscosity $(\eta/\eta^{o})^{1/3}$ *versus* complex to DNA concentration ratio ([complex]/[DNA]), where η and η^{o} represent DNA viscosity in presence and absence of complex, respectively [23].

2.5. *DNA interaction studies by UV–visible spectroscopy*

Commercial SSDNA was dissolved in distilled water and kept at 4 °C for less than 4 days. The nucleotide to protein ratio (N/P) greater than 1.8 was obtained from the ratio of absorbance at 260 and 280 nm (A_{260}/A_{280}), which indicated that the DNA was free from protein [24, 25]. The DNA concentration was calculated via absorption spectroscopy by using the molar absorption coefficient (ε) value of 6600 M^{-1} cm^{-1} (at 260 nm) for DNA [25] and was found to be 4.75×10^{-5} M. Working solutions were prepared from stock solution by dilution.

During the UV absorption titrations, concentration of complex was kept fixed while that of DNA was varied. Equivalent concentration of DNA was added to sample and the reference solution in order to eliminate absorbance of DNA. Before the absorption measurements complex-DNA solutions were kept as such for 30 min at room temperature. Absorption spectra were recorded in quartz cuvettes of 1 cm path length using a UV-1601 Shimadzu spectrophotometer at room temperature (25 ± 1 °C).

2.6. *Cyclic voltammetry*

Cyclic voltammetric measurements were performed on a SP-300 BioLogic Instrument, France. Measurements were carried out using a glassy carbon electrode (GCE) as working, a platinum wire (geometric area = 0.071 cm^2) as counter and silver–silver chloride as reference electrodes in a one-compartment electrochemical cell. The GCE was cleaned by polishing with alumina powder and rinsed with distilled water prior to the experiment to ensure a clean electrode surface. Measurements were carried out in aqueous DMSO (1 : 4) using KCl as supporting electrolyte. All experiments were performed at room temperature (25 ± 1 °C). At first, voltammograms were recorded in full potential window, i.e. −1.5 to +1.5 V, but the complexes showed peaks in the range of 0.0 to −1.5 V so the rest of the analysis was performed within the latter potential region.

2.7. *ALP inhibition activity*

The inhibition of ALP was measured by monitoring the rate of hydrolysis of *p*-NPP at 25 °C. Assay was prepared by using the same method, as reported earlier [26, 27] with slight modifications. Working substrate was made by mixing four parts of reagent A (diethanolamine pH 9.8, 2 M dm^{-3} and magnesium chloride 0.5 mM dm^{-3}) and one part of reagent B (*p*-nitrophenyl phosphate 50 mM dm^{-3}). Substrate was incubated for 5 min at 25 °C. In a cuvette, 2 mL of the substrate was taken and 40 µL of human serum having activity of 165 IU/L was added. After incubation for 1 min, absorbance was taken to check the activity of enzyme. ALP hydrolyzed the *p*-NPP and yellow *p*-nitrophenol was produced that absorbs at 405 nm as shown below,

$$p\text{-Nitrophenyl phosphate} + Mg^{+2} + H_2O \xrightarrow{ALP} p\text{-Nitrophenol} + Pi$$

where Pi is inorganic phosphate. Then various amounts of zinc complexes were added periodically from the stock solution (12.5×10^{-3} M, prepared in 1 mL of DMSO) and again incubated for 3 min. Absorbance was recorded again 1, 2, 3, 4 and 5 min thereafter. At the end their average was taken and % age inhibition calculated.

3. Results and discussion

3.1. *FT-IR data*

In IR spectra, difference of asymmetric and symmetric carboxylate stretching frequencies is often used as a spectroscopic criterion to determine the mode of carboxylate bonding [28]. In **1–3** the carboxylate showed νOCO_{asym} vibrations at 1527, 1599 and 1548 while νOCO_{sym} vibrations at 1359, 1364 and 1371 cm^{-1}, respectively. The calculated values of $\Delta\nu = [\nu OCO_{asym} - \nu OCO_{sym}]$ for **1** was 168 cm^{-1} showing bidentate carboxylate. The $\Delta\nu$ of 235 cm^{-1} for **2** shows monodentate coordination. For **3**, the calculated value of $\Delta\nu$ was 177 cm^{-1} indicating ionic carboxylate [6, 28]. The broad bands at 3500–2450 cm^{-1} for **1** and **3** are due to O–H of water involved in hydrogen bonding. The C–H stretches for aromatic were observed at 3081, 3003 and 3043 for **1–3**, respectively. The nitro of each of **1–3** gave two intense bands at 1486–1336 cm^{-1}. The vibrational bands at 1634, 1645 and 1642 correspond to C=C functionality, present in conjugation with aromatic moiety of **1–3**. For **3**, band corresponding to Zn–N appeared at 508 cm^{-1}. The absorption bands corresponding to Zn–O were observed at 425 and 420 cm^{-1} for **1** and **2**, respectively [29].

3.2. *NMR data*

^{1}H NMR chemical shifts of the ligand acid and its zinc(II) derivatives are given in table 1. For ligand the calculated values of coupling constants for H^2 and H^3 are 15.90 and 16.20 Hz, respectively, showing that ligand has *trans*-cinnamic unit. Upon complex formation, O–H signal of ligand at 12.69 ppm disappeared. The signals for olefinic protons shifted upfield. Signal of H^2 (7.69 ppm) and H^3 (6.75 ppm) shifted from their respective values to 7.47 and 7.21 and 6.74 and 6.61 ppm in **1** and **3**, respectively. Two signals for phenyl protons appeared at 7.90 and 8.21 ppm for **1** and at 7.76 and 8.18 ppm for **3**. The characteristic

Table 1. ^{1}H NMR data (ppm) of zinc(II) complexes with 4-nitrocinnamic acid (HL).

^{1}H	HL	$Zn(L)_2(H_2O)_2$ (**1**)	$Zn(en)_2(H_2O)_2](L)_2(H_2O)_2$ (**3**)
O–H	12.69	–	–
H^2	7.69 (d)	7.47 (d)	7.21 (d)
	[15.90]	[15.60]	[15.90]
H^3	6.75 (d)	6.74 (d)	6.61 (d)
	[16.20]	[16.20]	[15.90]
$H^{5,5'}$	7.97 (d)	7.90 (d)	7.76 (d)
	[8.70]	[8.10]	[8.70]
$H^{6,6'}$	8.23 (d)	8.21 (d)	8.18 (d)
	[8.40]	[8.40]	[8.70]
$H_{(water)}$	–	3.36 (s)	3.53 (s)
α	–	–	1.71 (s)
β	–	–	2.60 (s)

Notes: (d) = doublet, (s) = singlet. Values in square brackets show the [^{1}H,^{1}H] coupling in Hz.

peak at 3.36 ppm for **1** is clear indication of water attached to zinc. In **3**, two singlets are at 1.71 and 2.60 ppm for NH_2 and CH_2 protons of ethylenediamine, respectively. A singlet at 3.53 ppm in **3** indicates the presence of water (scheme 1).

3.3. *Single crystal X-ray analysis*

Crystal data and structure refinement parameters for **1–3** are given in table 2.

3.3.1. Crystal structure of 1. The molecular structure of **1** is shown in figure 1 and structure refinement parameters are given in table 2. Zinc(II) is coordinated by two carboxylates and two water molecules. Each carboxylate chelates zinc bidentate. The molecules crystallize in monoclinic crystal system with *C2/c* space group. The geometry around zinc is distorted octahedral, where the distortion can be due to electron pair repulsion and steric effects induced by carboxylate.

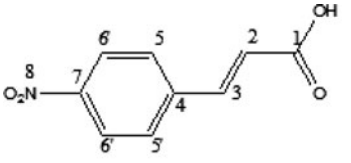

Scheme 1. Atom numbering scheme for the ligands.

Table 2. Structure refinement parameters for **1–3**.

Complex	**1**	**2**	**3**
Chemical formula	$C_{18}H_{16}N_2O_{10}Zn$	$C_{22}H_{24}N_2O_{10}S_2Zn$	$C_{22}H_{36}N_6O_{12}Zn$
Formula weight	485.70	605.92	641.94
T (K)	296(2)	296(2)	296(2)
Wavelength (Å)	0.71073	0.71073	0.71073
Crystal system	Monoclinic	Monoclinic	Triclinic
Space group	*C2/c*	*C2/c*	*P-1*
a (Å)	31.149(8)	27.753(2)	6.1220(5)
b (Å)	4.9797(11)	6.740(3)	7.4472(7)
c (Å)	12.128(3)	13.861(4)	15.6468(13)
α (°)	90	90	96.126(4)
β (°)	103.234(7)	91.901(3)	101.269(3)
γ (°)	90	90	90.264(3)
V (Å^3)	1831.2(8)	2591.4(14)	695.38(10)
Z	4	4	1
Absorption coefficient (mm^{-1})	1.407	1.166	0.955
F (0 0 0)	992	1248	336
Crystal size (mm)	0.30 × 0.20 × 0.16	0.30 × 0.24 × 0.22	0.30 × 0.24 × 0.22
θ-Range for data collection	2.687–26.00	1.468–27.879	1.335–27.99
Reflections collected	1801	3060	3330
Independent reflections	1140	2474	3110
Goodness-of-fit on F^2	0.994	1.024	1.056
Final R indices [$I > 2\sigma(I)$]	$R_1 = 0.0522$	$R_1 = 0.0353$	$R_1 = 0.0366$
	$wR_2 = 0.0976$	$wR_2 = 0.0891$	$wR_2 = 0.0920$
R indices (all data)	$R_1 = 0.1007$	$R_1 = 0.0478$	$R_1 = 0.0338$
	$wR_2 = 0.1157$	$wR_2 = 0.0972$	$wR_2 = 0.0901$
Data/restraints/parameters	1801/0/147	3060/0/216	3310/0/185

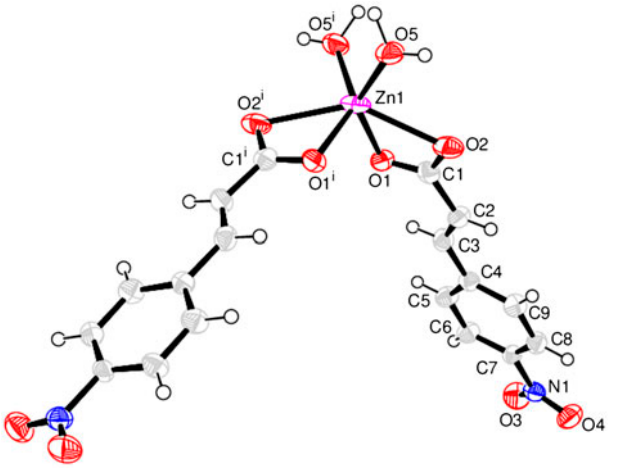

Figure 1. ORTEP diagram of **1** (i = $-x$, y, $-z+½$).

Table 3. Selected bond lengths (Å) and angles (°) of **1–3**.

	1	**2**	**3**
Bond lengths (Å)			
Zn–O1	2.044(3)	1.869(9)	2.2493(14)
Zn–O5	1.999(3)	1.9685(16)	–
Zn–O2	2.467(3)	–	–
Zn–N1	–	–	2.1264(15)
Zn–N2	–	–	2.139(15)
Bond angles (°)			
O1–Zn–O1	95.73(16)	84.0(5)	180.0
O1–Zn–O2	57.13(11)	–	–
O2–Zn–O5	81.11(12)	–	–
O2–Zn–O2	143.80(15)	–	–
O5–Zn–O5	95.60(2)	106.79(11)	–
O5–Zn–O1	99.86(13)	–	–
C1–Zn–O1	100.7(3)	–	–
Zn–O2–C1	81.7(3)	–	–
Zn–O5–H5A	122(4)	–	–
Zn–O5–H5B	120(3)	–	–
O1a–Zn–O5	–	109.05(3)	–
C1a–O1a–Zn	–	112.4(8)	–
S1–O5–Zn	–	123.68(9)	–
N2–Zn–O1	–	–	91.83(6)
N1–Zn–O1	–	–	88.82(6)
N1–Zn–N2	–	–	81.97(6)
N1–Zn–N1	–	–	180.00(9)
N2–Zn–N2	–	–	180.0
C1–N1–Zn	–	–	108.35(12)
C2–N2–Zn	–	–	106.99(12)

The asymmetric coordination of two carboxylates to the zinc center is reflected by a longer Zn–O2 (2.467 Å) and a shorter Zn–O1 bonds (2.044 Å). The longer Zn–O bond distances are accompanied by shorter C–O bond distances and vice versa. Selected bond lengths and angles of **1** are given in table 3.

Figure 2 depicts b-projection of **1** with infinite 2-D supramolecular network having base vectors [0 1 0] and [0 0 1] in the plane (1 0 0). The oxygens of carboxylate show H-bonding interactions with protons of water. The oxygens of nitro interact with phenyl protons.

3.3.2. Crystal structure of 2. The ORTEP diagram of **2** is depicted in figure 3. The zinc is four coordinate, chelated by four oxygens, one from each carboxylate and one from each DMSO. The carboxylates are monodentate. The complex has tetrahedral geometry around zinc, with O1–Zn–O5 bond angle equal to 109.05 Å. The crystal system is monoclinic with *C2/c* space group. The structure refinement parameters are given in table 2. The degree of

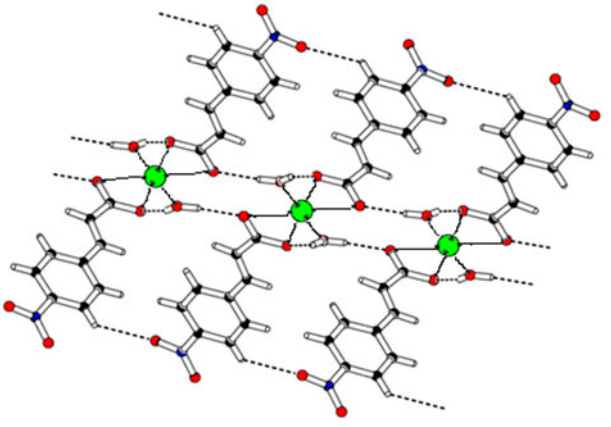

Figure 2. b-projection of **1**.

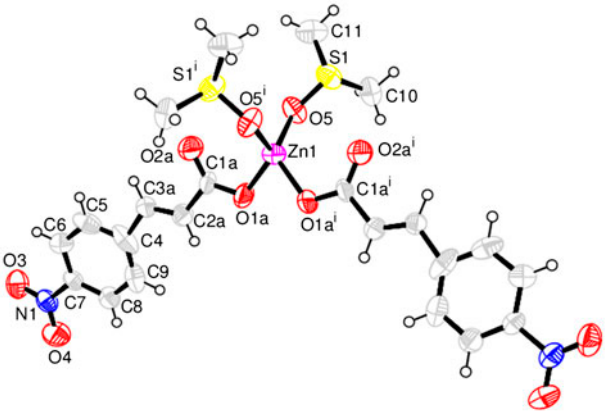

Figure 3. ORTEP diagram of **2** (i = $-x$, y, $-z+½$).

symmetry in Zn–O bond distance is the same for both carboxylate groups (1.869 Å). Similarly, Zn–O bond lengths are also the same for both DMSO groups (1.9685 Å).

The change in the bonding mode of carboxylate in comparison to that in **1** can be correlated to the presence of bulky DMSO. The two methyl groups attached to sulfur in addition to lone pairs of electrons present may cause steric hindrance which is reduced by changing binding mode of carboxylate from bidentate to monodentate. Selected bond lengths and angles for **2** are given in table 3.

Figure 4 shows H-bonding diagram of **2** where the packing is aided by the large number of interactions in which oxygen, nitrogen and hydrogen are involved. Protons of both methyl groups of DMSO are involved in intermolecular H-bonding. One methyl proton interacts with oxygen of carboxylate at 2.720 Å and the proton of the second methyl group interacts with oxygen of nitro from a neighboring molecule at 2.007 Å.

3.3.3. Crystal structure of 3. Figure 5 depicts the ORTEP diagram of **3** in which zinc is chelated by two ethylenediamine groups and binds two waters. Both ethylenediamine groups are bidentate. The geometry around zinc in the complex is octahedral and the crystal system is triclinic with *P-1* space group. The Zn–N bonds have different lengths in a

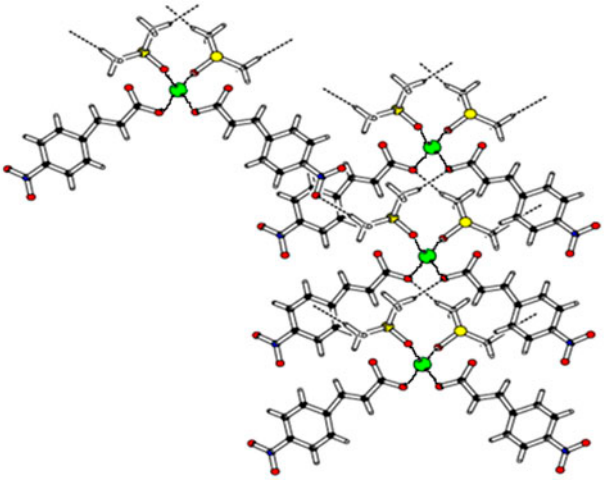

Figure 4. H-bonding diagram of **2**.

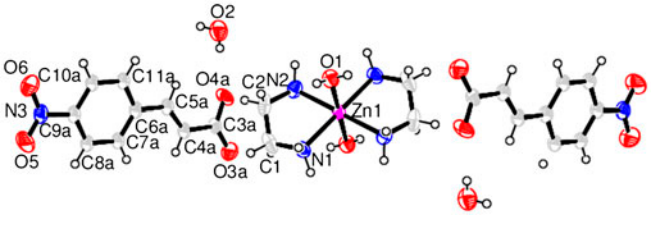

Figure 5. ORTEP diagram of **3** (i = $-x+1$, $-y$, $-z$).

slightly asymmetric geometry. Selected bond lengths and angles are given in table 3 and crystal structure refinement parameters in table 2. In **3**, ethylenediamine replaced carboxylate, present outside the coordination sphere. In addition, there are two water molecules present outside the coordination sphere which help form the supramolecular structure.

Figure 6 gives b-projection of **3**, which has an infinite 2-D supramolecular network with base vectors [1 0 0] and [0 1 0] in the plane (0 0 1). Oxygen, nitrogen and hydrogens are involved in H-bonding interactions.

3.4. *Viscosity measurements*

Viscosity measurements were performed to predict the mode of DNA binding. Viscometry is an effective tool to discern the DNA binding. The hydrodynamic measurements related to DNA viscosity are sensitive to variation in DNA chain length [30, 31]. This variation in viscosity serves as the least ambiguous method for DNA binding in solution. Figure 7 gives the plot of relative viscosity $(\eta/\eta^{o})^{1/3}$ *versus* complex to DNA concentration ratio ([complex]/[DNA]). The relative viscosity decreased on increasing concentration of complex, while keeping DNA concentration constant. This decrease in viscosity is indicative of electrostatic DNA binding mode and is similar to already reported zinc complexes [32].

3.5. *DNA binding studies by UV–visible spectroscopy*

The interaction of the synthesized complexes with DNA was also studied by UV–visible absorption spectroscopy to further explore the mode of interaction and the binding strength. Absorption titration experiments were performed keeping concentration of the complex constant and varying DNA concentration (2.26–20.34 μM). Upon incremental addition of DNA, change in spectrum occurs indicating some interaction between DNA and complex. The effect of different DNA concentrations on the electronic absorption spectrum of 0.25 mM solution of **1** and **2** is shown in figures 8 and 9, respectively.

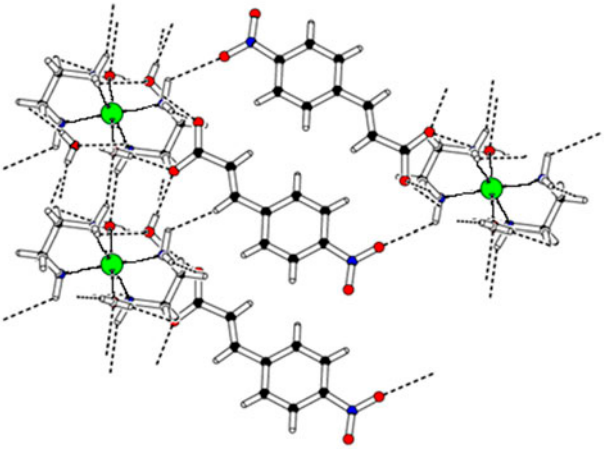

Figure 6. b-projection of **3**.

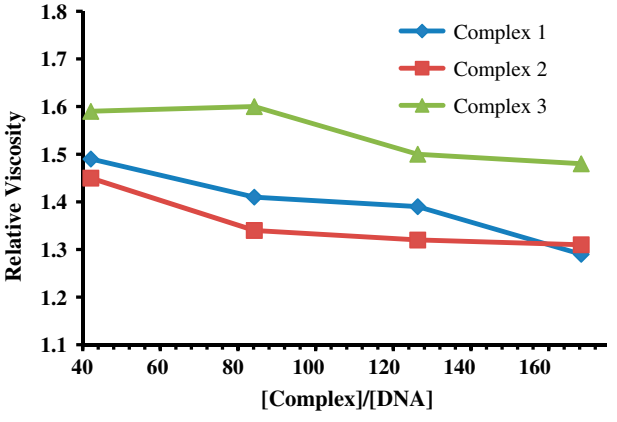

Figure 7. Effect of increasing amount of **1–3** on relative viscosity of DNA.

On increasing DNA concentration there was decrease in the absorbance i.e. hypochromism, for both complexes. The strong absorption of these complexes in the near UV (280–360 nm) is attributed to the long-lived triplet excited state of the aromatic moiety [18]. Upon increasing DNA concentration, along with hypochromism, blue shift

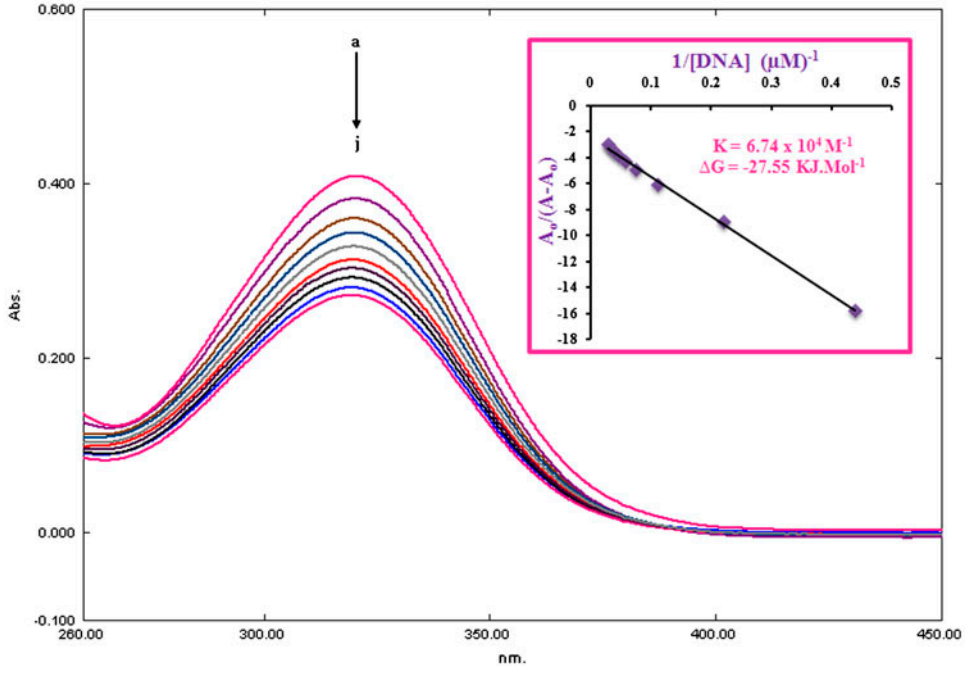

Figure 8. Absorption spectrum of **1** in the absence (a) and presence of 2.26 μM (b), 4.52 μM (c), 6.78 μM (d), 9.04 μM (e), 11.3 μM (f), 13.56 μM (g), 15.82 μM (h), 18.08 μM (i) and 20.34 μM DNA (j). The arrow direction indicates increasing DNA concentration.

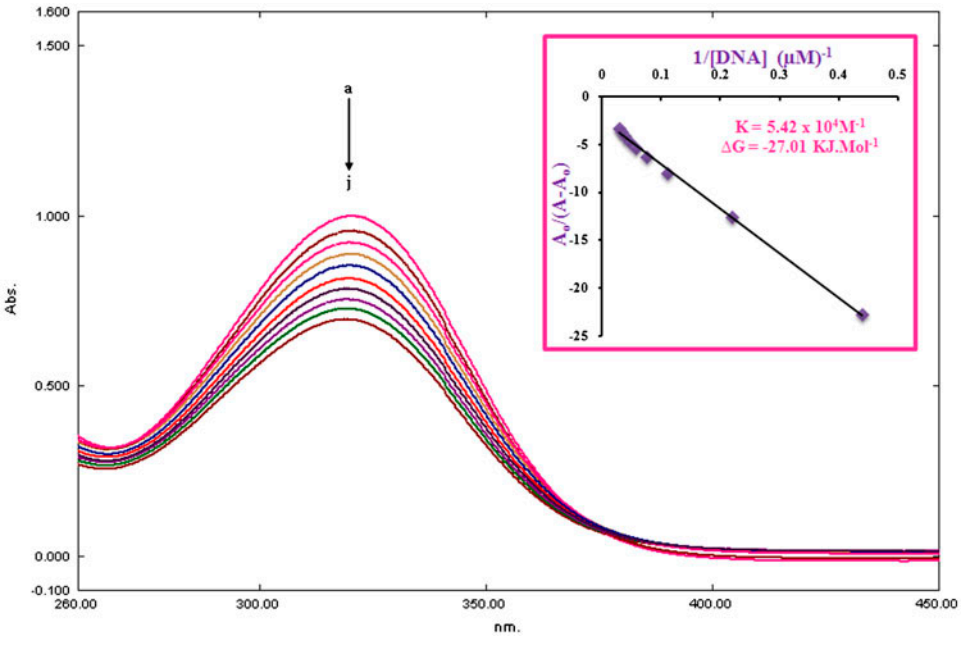

Figure 9. Absorption spectrum of **2** in the absence (a) and presence of 2.26 μM (b), 4.52 μM (c), 6.78 μM (d), 9.04 μM (e), 11.3 μM (f), 13.56 μM (g), 15.82 μM (h), 18.08 μM (i) and 20.34 μM DNA (j). The arrow direction indicates increasing DNA concentration.

(hypsochromism) of 1 and 2 nm was observed for **1** and **2**, respectively. These spectral changes show binding of the complexes to DNA. The hypsochromism and hypochromism are associated with double helical structure of DNA. Hypochromism is due to contraction of DNA helix along with other conformational changes [18, 33].

The blue shift shows electrostatic mode of DNA binding [18] and the nitro group in the complex is also involved in hydrogen bonding. So the suggested binding mode of DNA is electrostatic along with hydrogen bonding. Hydrogen bonding and other hydrophobic interactions between complementary bases in DNA strands are responsible for maintaining the helical structure of DNA. In the complex-DNA adduct, metal undergoes electrostatic interactions with the negatively charged phosphate groups in the DNA backbone. Meanwhile nitro group interferes by hydrogen bonding with DNA bases. Both these factors may unwind DNA double helix, collectively.

The binding constants of the complexes with DNA were calculated by using the Benesi-Hildebrand equation [18, 33],

$$\frac{A_o}{A - A_o} = \frac{\varepsilon_G}{\varepsilon_{H-G} - \varepsilon_G} + \frac{\varepsilon_G}{\varepsilon_{H-G} - \varepsilon_G} \cdot \frac{1}{K[\mathrm{DNA}]} \quad (1)$$

where K is binding constant, A and A_o are absorbances of complex-DNA adduct and pure complex, respectively, ε_{H-G} and ε_G are molar absorption coefficients of complex-DNA adduct and complex, respectively. Binding constants were calculated from the plot of 1/[DNA] along the abscissa and $A_o/A - A_o$ along the ordinate. The calculated values of

binding constants were $6.74 \times 10^4\,M^{-1}$ and $5.42 \times 10^4\,M^{-1}$ for **1** and **2**, respectively. The values of K_b are comparable to those determined for other zinc complexes [34–37].

The Gibb's free energy was calculated using equation (2) [38],

$$\Delta G = -RT \ln (K) \tag{2}$$

where R is general gas constant ($8.3141\,J\,M^{-1}\,K^{-1}$) and T is absolute temperature (298 K). The calculated values of Gibb's free energy change for **1** and **2** are −27.55 and −27.00 kJ M^{-1}, respectively. Negative value of ΔG indicate spontaneiety of the complex-DNA adduct formation.

3.6. *DNA binding studies by cyclic voltammetry*

In cyclic voltammetry, the changes in peak potential and peak current of the complex-DNA adduct in comparison to free complex were used to evaluate the DNA binding mode. The binding constant of the drug with DNA was determined from the diminution in the peak currents by using the following equation [39],

$$\log (1/[\mathrm{DNA}]) = \log K + \log (I/(I_o - I)) \tag{3}$$

where I_o is the peak current for free complex, I is the peak current for DNA bound complex and K is the binding constant. The diffusion coefficients were also determined for free complex and complex-DNA adduct by using Randles–Sevcik equation [40],

$$I_p = 2.99 \times 10^5 n(\alpha n)^{1/2} A C_o D_o^{1/2} \upsilon^{1/2} \tag{4}$$

where I_p is the peak current, C_o is the concentration of the complex ($M\,cm^{-3}$), A represents geometric area of the electrode (cm^2), n is the number of electrons involved in the redox process, D_o is the diffusion coefficient ($cm^2\,s^{-1}$) and υ is the potential scan rate (Vs^{-1}). The value of αn was calculated by using the following equation,

$$\left|E_p - E_p/2\right| = \frac{47.7}{\alpha n}\,\mathrm{mV} \tag{5}$$

where E_p and $E_p/2$ are the peak potential and half wave peak potential, respectively, n represents the number of electrons transferred in the rate determining step and α is charge transfer coefficient.

Complex **1** showed high electrochemical stability with three peaks in forward scan and same number of peaks in reverse scan in the potential range of 0.0 to −1.5 V as shown in figure 10(A). The oxidation and reduction maxima occurred at −0.267 and −1.045 V, respectively. To calculate the binding constant of **1** with DNA, change in the peak current was monitored on successive addition of DNA. Upon addition of 1 mL of 20 μM DNA, oxidation current of the free **1** (2 mM) suffered a reduction by 7 μA along with 81 mV shift in cathodic direction. This shift towards negative potential indicates strong electrostatic binding of the complex with DNA. The peak shift observed for the complexes is opposite to those observed for other zinc complexes already reported [41, 42]. The peak current was reduced as a result of decrease in the concentration of free **1**, which is due to formation of macromolecular **1**-DNA adduct, which diffuses slowly to the electrode surface. Similarly, on addition of 1 mL of 40, 60, 80 and 100 μM DNA to the separate solutions (same

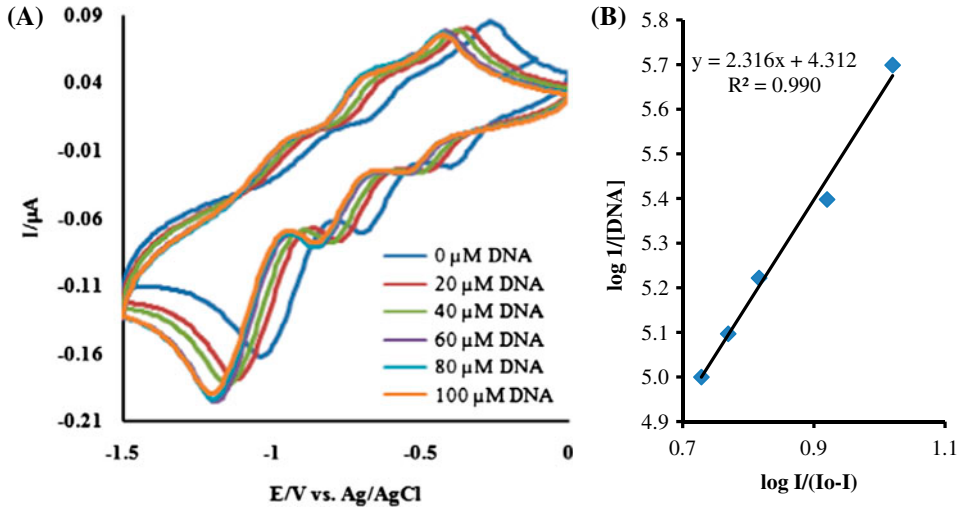

Figure 10. (A) Cyclic voltammograms of 2 mM **1** with 1 mL of 1.5 M KCl as supporting electrolyte in the absence and presence of 20, 40, 60, 80 and 100 μM DNA showing a decrease in current and a concentration dependent shift in potential. (B) Representative plot of log (1/[DNA]) *vs.* log $I/(I_o - I)$ for determination of binding constant.

concentration of the complex (2 mM) and supporting electrolyte) of free **1**, the peak current was reduced by 12, 19, 24 and 28 μA, respectively, with 10–30 mV negative shift in peak potential. Based on the reduction in peak current on DNA addition, the value of DNA binding constant was calculated from the intercept of log (1/[DNA]) *versus* log $I/(I_o - I)$ plot as shown in figure 10(B). The K_b value was $2.05 \times 10^4\ M^{-1}$ for **1**.

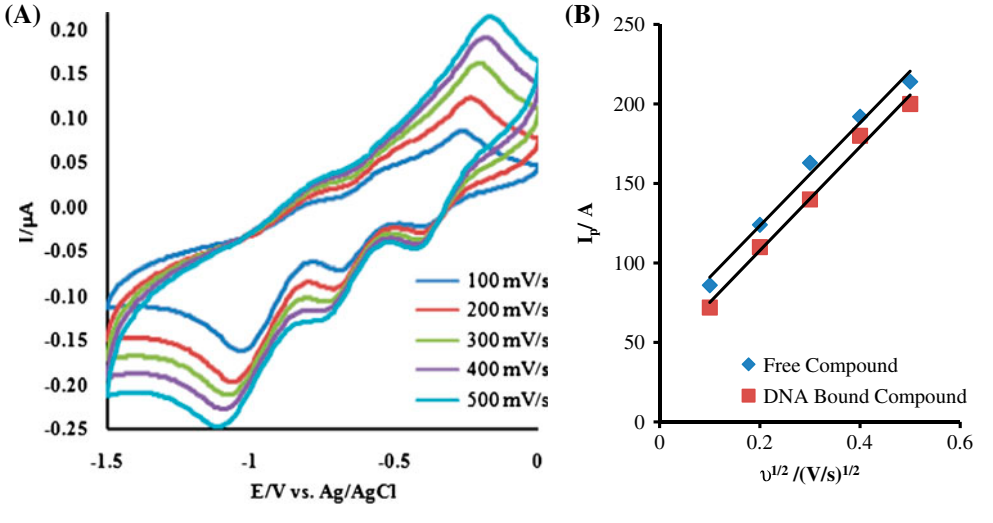

Figure 11. (A) Representative plots of I (μA) *vs.* E (V) (Ag/AgCl) at different scan rates for **1**. (B) Representative plots of I_p *vs.* $v^{1/2}$ for the determination of diffusion coefficient of free and DNA bound **1**.

The voltammograms of the free complex and its adduct with DNA (1 mL of 20 μM) were recorded at different scan rates up to 500 mV/s. These voltammograms of free complex at different scan rate are shown in figure 11(A). From the plot of I_p *versus* $v^{1/2}$ [figure 11(B)] the values of the diffusion coefficients for free and DNA bound complex were calculated using equation (4). The diffusion coefficient for the free complex, D_f (1.74×10^{-4} cm^2 s^{-1}) is higher than that for the DNA bound complex, D_b (1.71×10^{-4} cm^2 s^{-1}), indicating the formation of slowly diffusing supramolecular complex-DNA adduct on addition of DNA.

Complexes **2** and **3** also exhibited well-defined redox peaks in the potential region of 0.0 to −1.0 V. Similar to **1**, **2** and **3** showed negative shift in peak potential upon successive addition of DNA, which indicated electrostatic mode of DNA binding. DNA binding constants were calculated as 1.02×10^4 and 1.09×10^4 M^{-1} for **2** and **3**, respectively. The values of diffusion coefficients (D_o) in absence of DNA were calculated as 1.48×10^{-5} cm^2 s^{-1} for **2** and 1.07×10^{-5} cm^2 s^{-1} for **3**. These values are higher than those of their DNA-adducts (1.64×10^{-5} and 7.37×10^{-6} cm^2 s^{-1} for **2** and **3**, respectively), which can be attributed to formation of slowly diffusing supramolecular complex-DNA adducts in solution.

3.7. *ALP inhibition activity*

The synthesized complexes were also screened for their ALP inhibition activity. The activity of ALP was monitored in the absence and presence of inhibitor (complexes). The substrate used (*p*-nitrophenylphosphate) gives yellow *p*-nitrophenol upon hydrolysis. The concentration of *p*-nitrophenol is directly related to activity of inhibitor and was measured spectrophotometrically.

Figure 12 shows % inhibition of ALP by 4-nitrocinnamate ion (L) and its zinc(II) complexes. Ligand itself showed less than 20% inhibition of ALP, which can be correlated to the chelating ability of carboxylate to the active sites of the enzyme. The nitro group present on the aromatic system is analogous to that of the *p*-nitrophenylphosphate. Hence it may compete with *p*-NPP to occupy enzyme's active site and inhibit ALP. Among the complexes, **1** showed highest ALP inhibition, at 80% ALP inhibition at 1.2 mM concentration; activity can be attributed to release of zinc ions in solution. These released zinc ions not only occupy zinc binding sites but also Mg^{+2} binding sites at enzyme's surface, thus minimizing its activity [15]. Complex **2** showed approximately 40% inhibition of ALP, which is

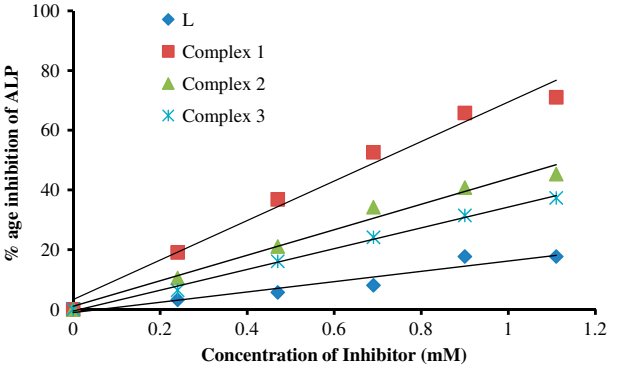

Figure 12. ALP inhibition profile by L and its Zn(II) complexes.

half of that shown by **1**. This decrease in activity is due to the presence of bulky DMSO in **2**. Complex **3** had lower activity which is related to its larger size. Greater bulk of complex makes its movement in solution difficult and also accommodation on enzyme's active site would be difficult. In short, all the complexes were active against ALP and activity is inversely related to size.

4. Conclusion

Three new O- and N-donor zinc(II) complexes have been synthesized and characterized by FT-IR, NMR and single crystal X-ray diffraction analysis, which confirmed distorted octahedral geometry for **1** and **3** and tetrahedral for **2**. The structures deduced by using FT-IR and NMR data were in agreement with those from single crystal X-ray analysis. DNA binding studies by using viscometry, UV–visible spectroscopy and cyclic voltammetry depicted electrostatic binding of these complexes with the negatively charged DNA backbone. Higher value of DNA binding constant for **1** can be related to its smaller size, which facilitates binding with DNA. Negative ΔG indicates spontaneous binding of complexes with DNA. The values of diffusion coefficients for all the synthesized complexes were higher when compared to their bulky DNA bound adducts. The synthesized complexes were also screened for ALP inhibition. Results showed that complexes are good inhibitors of ALP and inhibition is concentration dependent. Complex **1** showed greater inhibition related to its symmetrical structure and smaller molecular mass.

Supplementary material

Crystallographic data for the structures of the complexes reported in this article have been deposited with the Cambridge Crystallographic Data Center, CCDC # 965564–965566 corresponding to complexes **2**, **1** and **3**, respectively. Copy of the information may be obtained free of charge from The Director, CCDC, 12, Union Road, Cambridge CB2 1EZ [Fax: +44 (1223)336 033] or Email: deposit@ccdc.cam.ac.uk.

Acknowledgement

M.I. is thankful to the Higher Education Commission of Pakistan for providing scholarship.

References

[1] S. Caglar, S. Demir, Z. Heren, O. Büyükgüngör. *Polyhedron*, **30**, 1389 (2011).
[2] D. Dobrzyńska, T. Lis, L.B. Jerzykiewicz. *Inorg. Chem. Commun.*, **8**, 1090 (2005).
[3] M. Eddaoudi, D.B. Moler, H. Li, B. Chen, T.M. Reineke, M. O'Keeffe, O. Yaghi. *Acc. Chem. Res.*, **34**, 319 (2001).
[4] J. Moellmer, E.B. Celer, R. Luebke, A.J. Cairns, R. Staudt, M. Eddaoudi, M. Thommes. *Microporous Mesoporous Mater.*, **129**, 345 (2010).
[5] F. Natella, M. Nardini, M.D. Di Felice, C. Scaccini. *J. Agric. Food Chem.*, **47**, 1453 (1999).
[6] V. Zeleňák, I. Císařová, P. Llewellyn. *Inorg. Chem. Commun.*, **10**, 27 (2007).

[7] S. Adisakwattana, W. Sompong, A. Meeprom, S. Ngamukote, S. Yibchok-anun. *Int. J. Mol. Sci.*, **13**, 1778 (2012).
[8] I.M. Liu, F.L. Hsu, C.F. Chen, J.T. Cheng. *J. Pharmacol.*, **129**, 631 (2000).
[9] V. Zeleňák, M. Sabo, W. Massa, P. Llewellyn. *Inorg. Chim. Acta*, **357**, 2049 (2004).
[10] W. Kaim, B. Schwederski. *Bioinorganic Chemistry: Inorganic Elements in the Chemistry of Life — An Introduction and Guide*, John Wiley and Sons, Chichester (1994).
[11] B.L. Vallee, D.S. Auld. *Biochemistry*, **24**, 5647 (1990).
[12] E. Kimura, T. Koike. *Adv. Inorg. Chem.*, **44**, 229 (1996).
[13] S.C. Cunnane. *Zinc: Clinical and Biochemical Significance*, CRC Press, Boca Raton, FL (1988).
[14] O.M. Yaghi, M.O. O'Keeffe, N.W. Ockwig, H.K. Chae, M. Eddaoudi, J. Kim. *Nature*, **423**, 705 (2003).
[15] R.L. Dean. *Biochem. Mol. Biol. Educ.*, **30**, 401 (2002).
[16] M.R. Malik, V. Vasylyeva, K. Merz, N. Metzler-Nolte, M. Saleem, S. Ali, A.A. Isab, K.S. Munawar, S. Ahmad. *Inorg. Chim. Acta*, **376**, 207 (2011).
[17] C. Zhang, C. Janiak. *J. Chem. Crystallogr.*, **31**, 29 (2001).
[18] M. Sirajuddin, S. Ali, A. Haider, N.A. Shah, A. Shah, M.R. Khan. *Polyhedron*, **40**, 19 (2012).
[19] J.K. Barton. *Pure Appl. Chem.*, **61**, 563 (1989).
[20] J. Lu, X. Liao, B. Wu, P. Zhao, J. Jiang, Y. Zhang. *J. Coord. Chem.*, **66**, 1574 (2013).
[21] K.S. Shanmuga Bharathi, S. Sreedaran, A.K. Kalilur Rahiman, K. Rajesh, V. Narayanan. *Polyhedron*, **26**, 3993 (2007).
[22] G.M. Sheldrick. *SHELXS-97, Program for X-ray Crystal Structure Refinement*, Göttingen University, Göttingen (1997).
[23] J. Liu, T. Zhang, T. Lu, L. Qu, H. Zhou, Q. Zhang, L. Ji. *J. Inorg. Biochem.*, **91**, 269 (2002).
[24] M. Sirajuddin, S. Ali, A. Badshah. *J. Photochem. Photobiol., B*, **124**, 1 (2013).
[25] F. Asghar, A. Badshah, A. Shah, M.K. Rauf, M.I. Ali, M.N. Tahir, E. Nosheen, Z. Zia-ur-Rehman, R. Qureshi. *J. Organomet. Chem.*, **717**, 1 (2012).
[26] K.S. Munawar, S. Ali, A.N. Khan, S. Shahzadi, S.K. Sharma, K. Qanungo. *Inorg. Chem. Indian J.*, **7**, 82 (2012).
[27] German Society of Clinical Chemistry. *Z. Klin. Chem. Klin. Biochem.*, **10**, 281 (1972).
[28] V. Zeleňák, Z. Vargová, K. Györyová. *Spectrochim. Acta Part A*, **66**, 262 (2007).
[29] V.P. Singh, P. Singh. *J. Mol. Struct.*, **1035**, 363 (2013).
[30] H. Wu, Y. Bai, J. Yuan, H. Wang, G. Pan, X. Fan, J. Kong. *J. Coord. Chem.*, **65**, 2839 (2012).
[31] J. Lu, X. Liao, B. Wu, P. Zhao, J. Jiang, Y. Zhang. *J. Coord. Chem.*, **66**, 1574 (2013).
[32] D.-D. Li, Z.-W. Tao. *J. Coord. Chem.*, **66**, 4237 (2013).
[33] A. Shah, E. Nosheen, S. Munir, A. Badshah, R. Qureshi, Z. Rehman, N. Muhammad, H. Hussain. *J. Photochem. Photobiol., B*, **120**, 90 (2013).
[34] M. Jiang, Y.-T. Li, Z.-Y. Wu. *J. Coord. Chem.*, **65**, 1858 (2012).
[35] J. Lu, H. Guo, Y. Zhang, J. Jiang, Y. Liu, L. Zang, J. Huang. *J. Coord. Chem.*, **65**, 1765 (2012).
[36] Y.-F. Chen, M. Liu, J.-W. Mao, H.-T. Song, H. Zhou, Z.-Q. Pan. *J. Coord. Chem.*, **65**, 3413 (2012).
[37] Y.-G. Sun, K.-L. Li, Z.-H. Xu, T.-Y. Lv, S.-J. Wang, L.-X. You, F. Ding. *J. Coord. Chem.*, **66**, 2455 (2013).
[38] M. Sirajuddin, S. Ali, N.A. Shah, M.R. Khan, M.N. Tahir. *Spectrochim. Acta Part A*, **94**, 134 (2012).
[39] R.A. Hussain, A. Badshah, M.N. Tahir, B. Lal, I.A. Khan. *Aust. J. Chem.*, **66**, 626 (2013).
[40] M. Iqbal, S. Ali, N. Muhammad, M. Parvez, P. Langer, A. Villinger. *J. Organomet. Chem.*, **723**, 214 (2013).
[41] A.K. Asatkar, S. Nair, V.K. Verma, C.S. Verma, T.A. Jain, R. Singh, S.K. Gupta, R.J. Butcher. *J. Coord. Chem.*, **65**, 28 (2012).
[42] K. Pothiraj, T. Baskaran, N. Raman. *J. Coord. Chem.*, **65**, 2110 (2012).